Water in type I chondrules of Paris CM chondrite

A. Stephant, L. Remusat, F. Robert

Water in type I chondrules of Paris CM chondrite

A. Stephant[1,2*], L. Remusat[1] and F. Robert[1]

[1] Institut de Minéralogie, de Physique des Matériaux, et de Cosmochimie (IMPMC) Sorbonne Universités – Muséum National d'Histoire Naturelle, UPMC Univ Paris 06, UMR CNRS 7590, IRD UMR 206, 61 rue Buffon, F-75005 Paris, France.
[2] Center for Meteorite Studies, Arizona State University, Tempe, Arizona 85287-6004, USA

* Corresponding author: Alice Stephant: alice.stephant@gmail.com

Abstract

Hydrogen isotopic ratio and water concentration have been measured with the NanoSIMS in olivine, pyroxene and mesostasis phases in individual chondrules from the carbonaceous chondrites Paris (CM2), Renazzo (CR2) and ordinary chondrite Bishunpur (LL3). On average, chondrule pyroxenes in Renazzo, Bishunpur and Paris contain 893±637 ppm (1SD), 879±536 ppm and 791±227 ppm H_2O. Chondrule olivines from Renazzo and Bishunpur vary from 156±44 ppm to 222±123 ppm. Olivines in the Paris chondrules have high water concentration (603±145 to 1051±253 ppm H_2O) with a minimum mean value of 645±99 ppm. δD ranges from -212±125‰ to 15±156‰ and from -166±133‰ to 137±176‰ in Renazzo and Bishunpur chondrule olivines, pyroxenes and mesostases, respectively. In Paris chondrules, δD ranges from -398±23‰ to 366±35‰; this represents an extreme variation over 764‰. Paris olivines and pyroxenes are either enriched or depleted in deuterium relative to the mesostasis and no systematic isotopic pattern is observed. Simple model of chondrules hydration during parent body hydrothermal alteration is difficult to reconcile with such isotopic heterogeneity. It is proposed that a hydrous component, having a δD of c.a. -400‰, in the chondrule precursors, has been outgassed at 800-900°C in the gas phase. Nevertheless, a residual water fraction remains trapped in Paris chondrules. Quantitative modeling supports this scenario.

1. Introduction

Some carbonaceous chondrites (CC) hold hydrated minerals and contain up to 10 wt.% H_2O (Kerridge, 1985). They are the most plausible source of water delivery to the Earth (Marty, 2012; Walsh et al., 2011) as they display, on average, a similar D/H ratio as the Earth oceans, i.e. 155.76×10^{-6} (Robert, 2006). Thus, the carbonaceous chondrites are the key samples to constrain the origin of water on Earth. CM carbonaceous chondrites constitute an interesting class for studying aqueous alteration. Indeed, the CM chondrite group embraces type 1 (i.e. heavily aqueously altered) and type 2 (i.e. less aqueously altered) chondrites. Manganese-chromium dating of carbonates in CM chondrites gave a reliable aqueous alteration age of 4563.4+0.4/−0.5 million years (Fujiya et al., 2012); younger age than previous estimations (de Leuw et al., 2009). This CM carbonate age suggests the late onset of aqueous activities in the Solar System and allows Fujiya et al. (2012) to estimate that CM parent body accreted roughly 3.5 Myr after the birth of the Solar System.

Hydrated minerals and organic matter carry hydrogen in aqueously altered chondrites. Aqueous alteration of silicate minerals in these chondrites is evidenced by the occurrence of hydrous phyllosilicates, as serpentines, saponites, and smectites, which are the predominant phase in matrices of CCs (Garenne et al., 2014; Beck et al., 2010), often associated with carbonates and oxides (Howard et al., 2011) The petrologic chondrite classification reflects varying degrees of aqueous alteration in different groups of chondritic meteorites (Van Schmus and Wood, 1967). Classification of CMs is established based on a sequence of aqueous alteration (Alexander et al., 2013; Browning et al., 1996; Rubin et al., 2007).

Whether alteration on CM chondrite took place in the protosolar nebula or on the parent body is still a matter of debate: Ciesla et al. (2003) have argued for the hydration of silicate dust in the icy regions of the nebula during the passage of shock waves and Bishoff (1998) favors pre-accretionary alteration in the nebula, based on the relationship between fine-grained rims and their surrounding components. On the other hand, several observations support the hypothesis that the aqueous alteration occurred after the accretion onto the parent body (Brearley, 2003). For example, the existence of alteration zones, as Fe-rich aureoles around metal grains (Hanowski and Brearley, 2001), fluid inclusions (Fieni et al., 1978; Zolensky et al., 1999), supports this hypothesis. The oxygen isotopic data also indicate a parent body alteration: Young et al. (1999) explained the oxygen isotopic diversity of CC by simple down-temperature fluid flow within the parent body, based on the systematic relationships between the bulk oxygen isotopic composition of CC and the degree of aqueous alteration.

Chondrites show a systematic enrichment in deuterium relative to the molecular hydrogen of the protosolar nebula (Boato, 1954). The D/H ratio in matrix clays of chondrites has been assumed to reflect the D/H ratio of water that has circulated during the aqueous alteration of the parent body. Based on petrographic and mineralogical analyses in the heavily aqueously-altered Alan Hills 81002 CM2 chondrite, Hanowski and Brearley (2001) argued for the alteration of chondrules in a parent body environment. Nevertheless, hydrogen isotopic measurements performed on the Bishunpur and Semarkona LL3 ordinary chondrites and Renazzo CR2 carbonaceous chondrite showed large D/H heterogeneities among matrix clays and also between silicate minerals in chondrules (Deloule and Robert, 1995; Deloule et al., 1998). An isotopic reequilibration during hydrothermal alteration on the parent body by a homogenous aqueous reservoir cannot explain alone the heterogeneities of D/H ratio in these chondrites. D-enrichment of chondrite water could result from 2 scenarios (Bonal et al., 2013): (i) enrichment is an heritage of water formed in the outer solar system or presolar molecular clouds (Deloule and Robert, 1995; Deloule et al., 1998), variations observed in chondrites reflect different water reservoirs having different D/H ratios ; (ii) light water was formed in the warmer inner solar system and got enriched by secondary processes during aqueous alteration on the parent body including exchange with D-rich organics, oxidation of metal or other processes able to fractionate the initial D/H of water (Eiler and Kitchen, 2004; Alexander et al., 2012)

The CM2 Paris is a fresh sample that suffered only limited parent-body transformations, as revealed by preservation of amorphous silicates in the matrix. It is considered as the least altered CM chondrite currently known, classified as a CM2.7 (Hewins et al., 2014; Marrocchi et al., 2014). This sample offers a unique opportunity to study the initial stages of aqueous alteration on the CM parent body by investigating well preserved type I chondrules, which are not prone to aqueous alteration and are the least altered component in CM chondrites. Moreover, Paris exhibits heterogeneous alteration areas (Hewins et al., 2014), which bring us a large set of chondrules ranging from low to high alteration rate. Here we

investigated the water content and the D/H ratio in different phases (olivine, pyroxene and mesostasis) of 12 type I chondrules and the surrounding matrix from Paris. In comparison, 4 chondrules from Bishunpur (LL3) and 3 chondrules from Renazzo (CR2) were also analysed. Our aim was to determine if chondrules and matrix underwent the same aqueous alteration, by using the D/H ratio, or if they were subjected to different hydration episodes. The high lateral resolution of NanoSIMS allows measuring water content and hydrogen isotopic ratio in contiguous olivine, pyroxene and mesostasis of chondrules.

2. Samples

2.1. Objects of study

The Paris chondrite is a breccia with varying degrees of alteration and thus it contains both well preserved and altered chondrules. Three sections were analyzed in three sessions: one mounted in epoxy (i.e. Session I- chondrules 4, 6, 9, 19, 24 and 27) and two epoxy-free (i.e. Session II: chondrules 1 and 7; Session III: chondrules A, B, D and E). The latest were chosen to assess vacuum issues on the hydrogen contamination in addition to the effect of epoxy -expected to impregnate the sample at a fine scale- that could bias our measurements (Aubaud et al., 2007; Hauri et al., 2006; Stephant et al., 2014). The three sections of Paris were used for D/H analyses but only the one of session III were used for water content measurements. Renazzo and Bishunpur, mounted in epoxy, were also analysed as they exhibit heterogeneities of the D/H ratios in their chondrules, documented by previous studies (Deloule and Robert, 1995; Deloule et al., 1998) (i.e. Session IV – chondrules X, Y, Z and I, J, K, L). As such, they are used as references in this study. Renazzo is a CR2 chondrite which contains abundant type I chondrules (Weisberg et al., 1993) with intermediate level of alteration, evidenced by the replacement of chondrule mesostases by phyllosilicates. Bishunpur is a LL3.1 ordinary chondrite whose aqueous alteration was limited to the production of smectite in the matrix (Alexander et al., 1989). Type I chondrules were imaged using a JEOL JSM 840-A SEM installed at MNHN. Chemical characterization of olivine and pyroxene from 6 Paris chondrules (in the epoxy mount) were carried out using a CAMECA SX-100 EMPA at the Camparis facility, in Paris, France.

Paris contains markedly more type I than type II chondrules and their size ranges from ~100 to ~500 µm. In addition, type I chondrules in Paris have various petrologic characteristics. We selected 12 chondrules of different textural types and various degrees of aqueous alteration in order to survey the range of chondrules present in Paris. Backscattered electron images of these 12 chondrules are presented in Figure 1 to illustrate this diversity: barred olivines (chondrules 19, 24 and 1), radial pyroxene (chondrule 4), and porphyritic chondrules. Degree of chondrule aqueous alteration is established on the amount of metal globules, glassy stage of mesostasis and presence of alteration aureole. Moreover, various degrees of aqueous alteration are observed in chondrule mesostasis. For instance, chondrule 19 is a well-preserved object with glassy mesostasis and metal globules whereas chondrule 27 exhibits an altered mesostasis in its center and lacks of Fe-rich globules (Fig.1). X-ray elemental maps obtained by EDX allow us to select the target areas for NanoSIMS analysis; we aimed at areas with contiguous occurrences of olivine, pyroxene and mesostasis. The EMPA measurements (Table 1) indicate that all olivines type I chondrules from Paris are magnesium-rich (Fa<2). Low-Ca pyroxenes show limited compositional range (Fs ranges from 0.7 to 17.5; Wo ranges from 0.4 to 5.9 with an exception at 38.3). We also chose 4 representative type I chondrules in Bishunpur and 3 in Renazzo.

2.2. Standards

Silicate standards were used for calibration of water contents and for instrumental mass fractionation on D/H ratio. These standards match different phases analyzed in chondrules: pyroxene KBH1, olivine KLV-23, glass DR15-1-5, glass DR20-1-1, amphibole Mont Emma and amphibole Kipawa (Clog, 2010; Deloule, 1991; Koga et al., 2003). Their chemical compositions are reported in Table 2. Samples were mounted in such a manner to reduce a contribution of epoxy to the OH signal while having a nice polished surface: holes were drilled in a 10 mm aluminium disk with a 2 mm diameter drill bit. In each hole, samples were mounted individually with epoxy and then polished down to 0.25 µm diamond paste. Mounts were carbon-coated, thickness 20 nm. Chondrites and standards were outgassed for one week in the NanoSIMS airlock before each analytical session.

3. Methods

3.1 Quantification of water content

Elemental measurements were performed with the Cameca NanoSIMS 50 at MNHN, Paris. $^{16}OH^-$, $^{28}Si^-$, $^{24}Mg^{16}O^-$ and $^{27}Al^{16}O^-$ secondary ions were imaged and quantified using a Cs^+ primary beam. Special care was dedicated to correct the contribution of water contamination: we analyzed consecutively the same areas with two different primary beam intensities, 1.2pA and then 15pA, in order to estimate the part of OH contamination (Stephant et al., 2014). Indeed, using a correlation between the primary beam intensity and the OH^-/Si^- ratio, we calculated the OH^-/Si^- at the "infinite" primary beam intensity, supposed free of any OH contamination (see supplementary information for raw data). The primary beam was rastered over a 20×20µm² surface area divided in 256×256 pixels with a 200µm aperture diaphragm for 60 cycles. The counting time was set to 1ms/px. Prior to the analysis, a 25×25µm² surface area was presputtered for 20 minutes using a high primary beam current (i.e. 280pA and 230pA for the session III and IV, respectively) and a 750µm aperture diaphragm. The mass resolution power was ~6100 for $^{16}OH^-$ and ~7500 for $^{28}Si^-$ using the entrance slit ES3 and the aperture slit AS2. 39 areas were imaged in type I chondrules from Paris during session III, 14 from Bishunpur and 11 from Renazzo during session IV. Vacuum in the analytical chamber was 9.3×10^{-10} Torr for session III and 1.1×10^{-9} Torr for session IV.

Water concentrations in the different phases of chondrules were obtained using a calibration of OH^-/Si^- versus water concentration; water concentration is reported as [H_2O] and represents H_2O ppm /SiO_2wt. %. The calibration lines were forced to the origin: using our method to estimate the OH^-/Si^- ratio at infinite primary beam intensity, the surface contamination contribution on the OH^-/Si^- value is withdrawn (see the discussion of this calibration in Stephant et al., 2014). Different calibrations were used depending on the silicate mineralogy (Tenner et al., 2009) (Fig. 2): matrix effects are so strong that ferromagnesian minerals and amphiboles show similar OH^-/Si^- ratios for very distinct water concentrations (less than 200 ppm up for the former to compare with 1 wt. % for the latter). Thus it is crucial to precisely identify each analyzed mineral to accurately quantify its water content. To this end, $^{24}Mg^{16}O^-/^{28}Si^-$ and $^{27}Al^{16}O^-/^{28}Si^-$ are used to decipher between olivine, pyroxene and mesostasis (see supplementary information). Standard measurements for each session of analysis (i.e. III and IV) are reported in supplementary information. Uncertainties for each calibration line were evaluated using a code written on the R program (Thomen et al., 2014). The reported errors on meteorite measurements are dominated by uncertainties on the calibration slopes. The counting statistics on the OH^-/Si^- ratio are negligible compared to the calibration slope uncertainties.

3.2 Hydrogen isotopic ratios

Hydrogen isotopic measurements were performed by imaging H^- and D^- over the same areas studied for elemental analyses to provide both isotopic and elemental data at exactly the same location. Thereby, D/H images could be superimposed on elemental images. The primary beam was rastered over a 20×20µm² surface area divided in 256×256 pixels with a 300µm aperture diaphragm for 60 cycles with a counting time set to 1ms/px. The primary beam intensities was ~200-240pA for the three sessions on Paris chondrite and 29pA for the session IV (i.e. Bishunpur and Renazzo). Prior to each analysis, a 25×25µm² surface area was presputtered for 5 minutes using a high primary beam current (i.e. 230-280pA) with the 750µm aperture diaphragm. The entrance and the aperture slits were both set at the position 1. The instrumental isotopic fractionation factor for hydrogen was determined with the set of silicate standards previously described at each session (supplementary information). During sessions I, II and III, no matrix effect was noticed for the D/H ratio using NanoSIMS at the precision of our measurements (Hu et al., 2015). However, in the session IV, a significant difference in the instrumental isotopic fractionation was observed for the amphibole and the glass standards. That can be due to the lower primary beam intensity during this session compared to the three prior sessions. The instrumental isotopic fractionation factor was also calculated as the average of these standards. The uncertainty on the instrumental isotopic fractionation corresponds to the standard deviation of terrestrial standards (see supplementary information). Errors at the 2σ level (quadratic sum) combine the uncertainty on the instrumental mass fractionation factor and the counting statistic error on each measurement (dominated by the total number of counts detected for D^-). The D/H ratios are expressed in δ units (where $\delta D=[(D/H_{sample})/(D/H_{SMOW})-1] \times 1000$).

4. Results

4.1 Water concentration in nominally anhydrous minerals (NAMs)

Distribution of water concentrations in olivines and pyroxenes of type I chondrules (Table 3) are presented in Figure 3 for each chondrite. Mean water concentrations in pyroxenes are 893±637 ppm (1SD, n=4), 879±536 ppm (1SD, n=11) and 791±227 ppm (1SD, n=8) for Renazzo, Bishunpur and Paris, respectively. In olivine, water concentration varies markedly between Renazzo, Bishunpur and Paris: 156±44 ppm (1SD, n=7), 222±123 ppm (1SD, n=7) and 860±132 ppm (1SD, n=14), respectively. Relative uncertainties for these measurements are ±25% for Paris NAMs and ±50% for Bishunpur and Renazzo NAMs (supplementary information). It must be noted that significant uncertainties in the determinations of the water content in NAMs are due to the fact that our standards – being terrestrial nominally anhydrous minerals - have much lower water concentrations than those measured in Paris chondrules. This implies a large extrapolation towards large values hence larger uncertainties. Using the uncertainties on the NAMs water calibration line, the lowest estimations for pyroxene mean water concentrations become 447±318 ppm, 439±268 ppm and 557±147 ppm for Renazzo, Bishunpur and Paris, respectively. Regarding the olivines, the lowest estimations for mean water concentrations are 78±22 ppm, 111±61 ppm and 645±99 ppm, for Renazzo, Bishunpur and Paris, respectively. Therefore, Paris olivines appear to be more hydrated than those in Bishunpur and Renazzo chondrules and do contain a significant amount of water for a nominally anhydrous mineral. For pyroxenes, Bishunpur and Renazzo exhibit a more scattered distribution than Paris. The small numbers of chondrule analyzed for Bishunpur (i.e. 4) and Renazzo (i.e. 3) compared to Paris doesn't allow us to make a robust statement on the water content of these two meteorites. Moreover, water concentrations in Paris chondrules were determined in epoxy-free sections

(session III), allowing us to rule out a significant contribution from the epoxy in the OH^- signal and a subsequent bias in the determination of the water content (Aubaud et al., 2007).

4.2 Hydrogen isotopic ratio in chondrules

4.2.1 Comparison between Paris, Renazzo and Bishunpur

Distribution of the hydrogen isotopic composition of minerals in chondrules in Paris, Renazzo and Bishunpur (Table 3) are shown in Figure 4. The mean δD value for these three meteorites fall within the terrestrial domain (Lécuyer et al., 1998). Paris exhibits a wide spread of δD from -398±23‰ to 366±35‰ (i.e. covering a range of 764‰) with a mean value of -88±141‰ (2SD, n=70). In Paris, the δD of the surrounding matrix is -69±32‰. The possible contamination of the Paris samples by terrestrial moisture can be ruled out since chondrules show both enrichment and depletion of deuterium relative to the terrestrial value. The Paris mounts without epoxy (i.e. session II and III; chondrules A, B, D, E, 1 and 7) shows the largest range of δD values. In Renazzo, the δD in olivines, pyroxenes and mesostases range from -212±125 to 15±156 ‰ with a mean value of -131±115‰ (2SD, n=21). An image recorded in the matrix gives a value of 316±202‰. These determinations are consistent with previous studies in Renazzo (Deloule and Robert, 1995) showing that the matrix is enriched in deuterium (-37 to 733‰) relative to chondrules (-294 to 284‰). Bishunpur minerals range from -166±133‰ to 137±176‰ with a mean value of -66±148‰ (2SD, n=16). This range is significantly smaller compared to previous studies on Bishunpur chondrules: -371‰ < δD <1934‰ (Deloule and Robert, 1995; Deloule et al., 1998). We will focus our attention in the upcoming discussion on the emblematic case of Paris for which the δD variations reach 764‰.

4.2.2 Inter-chondrule variations in Paris

A broad inter-chondrule isotopic distribution is observed in Paris: in the mesostasis -292±32‰ <δD<366±35‰ with a mean value δD=-44±346‰ (2SD, n=26), in olivines -398±23‰ <δD<76±36‰ with a mean value of -136±258‰ (2SD, n=24) and in pyroxenes -342±23‰ <δD < 155±53‰ with a mean value of -84±250‰ (2SD, n=20). The δD in Paris chondrules spans over a range of 764‰; this corresponds to a large isotopic fractionation that is never observed in terrestrial samples. Pyroxenes and olivines exhibit the same range. Mesostasis seems to be slightly enriched in deuterium compared to adjacent olivine and pyroxene. However, individual chondrules exhibit more complex variations as discussed hereafter.

4.2.3 Intra-chondrule variations in Paris

In addition to the broad range of δD observed among chondrules, intra-chondrule heterogeneities are also pronounced in Paris. Indeed, an isotopic variation of 658‰ is observed between the different phases of the chondrule E and up to 664‰ for the chondrule A. More surprisingly, isotopic variation among olivines in chondrule A reaches 454‰ in less than ~200 µm. In Figure 5, NanoSIMS images of AlO^-/Si^- and D/H of a 20×20µm² area in the chondrule A are shown. Olivine and mesostasis that are contiguous exhibit a difference in δD of 317‰ with no visible gradient (the NanoSIMS resolution does not exceed ~500nm). In most cases, the mesostasis is enriched in deuterium compared to olivine and pyroxene (chondrules A, B, D, E, A, 7, 9) with the exception of chondrules 24, 6 and 27. As such, no systematic between mesostases δD and silicates δD is observed, suggesting there is no equilibrium between mesostasis and silicates

minerals. Futhermore, no correlation is observed between the degree of aqueous alteration experienced by the chondrule, as revealed by its petrology, and the δD distribution of the chondrule. In the less altered chondrule (19), there is no variation, within errors, of the δD value between the mesostasis and olivine and pyroxene (i.e. -34±79‰ on average, 2SD). However, chondrules A, E and 7 exhibit a low degree of aqueous alteration illustrated by abundant metal grains and they show a large isotopic heterogeneity between their minerals. In addition, chondrule 27 is heavily altered (its mesostasis is altered into phyllosilicates) while δD variations do not exceed 232‰ between mesostasis and minerals. An important point to notice is that chondrules A, E and 1, showing the largest range of δD values, were all measured in epoxy-free mounts. As a conclusion of this isotopic survey, δD variations are intrinsic to each chondrule but not related to their degree of aqueous alteration.

5. Discussion

5.1 Implication of the δD distribution for chondrule formation models

5.1.1 δD fractionation among coexisting minerals

The isotopic fractionation coefficient α between two phases corresponds to the ratio of their D/H values. Figure 6 reports the isotopic fractionation coefficients α between olivine and mesostasis versus those between pyroxene and mesostasis, reported as $10^3 \times \ln\alpha$ in per mil. Fractionation coefficients are calculated for adjacent phases (see supplementary information). Therefore, each point corresponds to a NanoSIMS image containing the 3 phases in a 20×20µm² surface area. A trend is observed with both positive and negative values. The slope of the correlation is not far from unity, indicating that pyroxene and olivine have similar δD. The important point to notice is the large range of fractionation coefficient values (i.e. $10^3 \times \ln\alpha$ ranging for -431‰ to +283‰). This correlation requires a process that would generate a large fractionation factors between minerals during chondrule history. Furthermore, this correlation has no link to the degree of aqueous alteration and is not simply related to hydrothermal alteration, which may imply that chondrules followed different fractionation history.

5.1.2 Low-temperature and hydrothermal alteration on the parent body under isotopic equilibrium conditions

The observed fractionation factors are too large to account for an isotopic fractionation at equilibrium during H isotopic exchange between H-bearing minerals and water. Significant intra-chondrules heterogeneities among the same phases are up to 764 ‰. In terrestrial environments, such variations are never observed among alteration products and fractionation factors between minerals and water are restricted to 60‰ (Saccocia et al., 2009). This should be regarded as clear evidence against a simple equilibrium isotope fractionation between phases of the same chondrule.

5.1.3 Modelling the chondrule alteration by an isotopically homogeneous fluid.

NAMs (i.e. olivine and pyroxenes) are either enriched or depleted in D relative to the mesostasis (Fig. 6). This suggests there is no equilibrium between mesostasis and these minerals. This results in a crossover rarely observed in natural environment, which should be regarded as a dependable constraint for chondrules formation models. We first discuss common geochemical situations that cannot yield such a crossover.

The progressive isotopic re-equilibration of the minerals with the mesostasis by diffusion of an external fluid to the chondrule cannot account for the isotopic crossover observed in the Figure 6 since isotopic fractionation will be unidirectional (Kyser and O'Neil, 1984). In other terms, the expected correlation for diffusion in the Figure 6 is either enriched or depleted relative to 0 but never on both sides.

However, we considered here diffusion by a reservoir of water with homogeneous isotope composition. Bonal et al. (2013) have shown that the δD of the matrix water is highly heterogeneous at the micrometer scale in CR chondrite. Piani et al. (2015) have shown that water-ice precursors with a large range of δD compositions could have accreted into the parent body and been responsible for matrix δD heterogeneities at the micron scale. Secondary processes on the parent body have also been suggested to explain this spatial variability (Alexander et al., 2010; Alexander et al., 2012). This δD spatial heterogeneity at a small scale could potentially have induced the heterogeneities observed among single chondrules. However, this model holds three issues. (1) The fractionation coefficients between ferromagnesians (i.e. olivine and pyroxene) and mesostasis show significant variations (cf. Fig. 6). This means that the δD of the mesostasis can be distinct from that in the pyroxene or olivine next to this mesostasis. Even if the aqueous alteration occurs at the micrometer scale, phases having common boundaries should record a similar δD value; plus or less the isotopic fractionation at equilibrium between phases (Saccocia et al., 2009). (2) The δD measured in the matrix covers a more restricted range (i.e. -66±70‰; 2SD) compared to the broad distribution of δD in chondrule phases; (3) This model does not account for the high water content in olivines, as it seems quite unrealistic to incorporate a minimum of 645 ppm H_2O inside an olivine at chondritic parent body conditions of pressure and temperature. This problem will be discussed in the next section.

Hence, hydration of the chondrule by parent body water does not fit the requirements to explain the isotopic crossover observed in the Figure 6. However, as shown in the next section, it may be explained by the evaporation of H before the formation of the parent body, provided that this H was present in chondrules at the moment of their formation.

5.2.3. Loss of H from chondrules during their cooling in the gas phase.

Here we propose that distillation of H took place during the melting and the cooling of the chondrule in the gas phase. This outgassing model has two implications: (1) the initial [H] concentration and (2) the degree of distillation caused by H_2 escape can vary from chondrule to chondrule. As the analyzed chondrules show various textural and petrological features, there is no reason that they share common initial water content and that they underwent the same degree of distillation.

Rayleigh distillation induced by the loss of H_2 from melted chondrules can be written as:

$$D/H(t)_{phase} = D/H(0)_{phase} \times f_{phase}^{(\alpha_{(H2-H2O)}-1)}$$

With D/H(0) the initial hydrogen isotope ratio of the mineral; D/H(t) the hydrogen isotopic ratio at instant t and f_{phase} is the remaining fraction of H in the mineral (i.e. from 1 to 0); α_{H2-H2O} is the isotopic fractionation between H_2 and H_2O in phases. The lowest measured value on chondrule phases i.e. for δD= -398‰ is used to set $D/H(0)_{phase}$. We assume that each phase follows its own *f* Rayleigh coefficient i.e.

that NAMs and mesostasis evolve independently since they do not share the same level of advancement of the diffusion for H species (Ingrin and Blanchard, 2006) and initial water concentration. Indeed, mesostasis can be either depleted or enriched relative to olivine and pyroxene, function of their relative degree of degassing. Calculations are reported in Figure 6 for f_{phase} values randomly generated for mesostasis and for NAMs. These calculations reproduce the wide range of isotopic fractionation variations with α_{H2-H2O} value of ≈0.9 for olivine and pyroxene and ≈0.85 for mesostasis. These α values are markedly different from unity and therefore consistent with the large H_2-H_2O isotopic fractionation factor (Simon et al., 2011). From these α values, we calculate a reducing temperature of the system during the isotope fractionation around 900-1100 °C (Simon et al., 2011).

An alternative scenario could involve the reduction of water during parent body processes (Alexander et al., 2010). Lécluse and Robert (1994) showed that the isotope exchange between H_2O and H_2 is still fast down to 200-300°C, i.e. at hydrothermalism temperatures. If we consider that a distillation took place around 150°C in the parent body (Clayton and Mayeda, 1999; Guo and Eiler, 2007), the fractionation factor between H_2 and H_2O should be far (α_{H2-H2O}≈0.3, by extrapolating from Simon et al., 2011) from our calculated value (α_{H2-H2O}≈0.9). In other terms, it seems unrealistic to argue that water reduction took place on the parent body while the hydrogen isotopic system registered temperatures around 900-1100 °C. We thus propose that chondrules have degassed their juvenile water prior to their incorporation in their parent body, presumably in the nebula, following the reduction of their water at temperature around 900-1100°C.

The lack of correlation between water content and the δD demonstrates that each chondrules contained heterogeneous initial water concentrations or δD or both. As analyzed chondrules are of different textural types, we can assume that each chondrule gets its own initial water content.

5.2 Incorporation of high water contents in NAMs

5.2.1 Data on Earth

It is now established that nominally anhydrous minerals are a major host for water in terrestrial mantle (Bell and Rossman, 1992; Bolfan-Casanova, 2005; Hirschmann et al., 2005; Peslier, 2010). Martin and Donnay (1972) were the first to propose a water incorporation model based on OH ions replacing O in the structure of pyroxenes. Water storage has been extensively studied in NAMs. Natural pyroxene water concentrations range from few 10s up to ~1100 ppm of H_2O, depending on the geological occurrence (Rauch and Keppler, 2002; Skogby, 2006; Sundvall and Stalder, 2011). Natural olivine contains significantly less water than pyroxene with contents ranging roughly between few and 400 ppm of H_2O (Bell and Rossman, 2003; Beran and Libowitzky, 2006). Measured water concentrations in NAMs of Paris chondrules (mostly olivines) are markedly higher than those in terrestrial ones. Thus water contents measured in olivine seem too high to come only from water in olivine.

However, several experiments show that olivine can incorporate significant amount of water at high pressure, high temperature (Kohlstedt et al., 1996; Mosenfelder et al., 2011; Ohtani et al., 2001). Férot and Bolfan-Casanova (2012) measured olivine water contents of 4690±1655 ppm for experiments performed at 9 GPa and 1175 °C. Smyth et al. (2006) found water solubility in olivines up to 8900 ppm at 12 GPa and 1250°C.

OH-rich inclusions in olivines and pyroxenes of magmatic origin could account for the large content we determine. For instance, Khisina et al. (2001) have shown that hydrogen incorporation in olivine exists in two modes: intrinsic mode into olivine structure (Wright, 2006) and extrinsic incorporation as nanometer-sized inclusions of OH bearing silicates. In pyroxene, hydroxyl can occur in the form of narrow lamellae of amphibole (Skogby et al., 1990; Veblen and Buseck, 1981).

5.2.2 Implications for chondrule olivines of Paris

From the experimental data on Earth's olivine, the striking water contents measured in Paris olivines could suggest that olivines were formed at high-pressure, high-temperature conditions in order to incorporate such amount of water; assuming that this water is under the form of hydroxylated groups in the structure of olivines. The model proposed by Libourel and Krot (2007) suggested that olivines are inherited from mantle planetesimals fragmented by impacts. In this scenario, mantle olivine can incorporate large amounts of water under conditions of high pressure and high temperature. As suggested by Libourel and Krot, pyroxenes could result from the destabilization of olivine caused by the incorporation of SiO diffusing from the gas phase. Qualitatively, this model accounts for the similar δD values in the pyroxene and in its parent olivine. Nevertheless, there are restrictions to this hypothesis. First, this scenario by Libourel and Krot is based on chondrules having a granoblastic texture that is not found in all our studied chondrules. Secondly, the kind of high pressure needed to incorporate a minimum of 645 ppm of water in olivine seems difficult to reconcile with a small parent body.

The speciation of hydrogen is not known through NanoSIMS analyses and it is limited by its spatial resolution (100nm). Nanometer-sized inclusions cannot be identified by NanoSIMS imaging. We assumed that the hydrogen occurs under the form of hydroxylated groups in the chondrule olivines. However, glass inclusions in olivines can be found in any type of chondrules (Varela et al., 2002; Florentin et al., 2016). These inclusions occur at the micrometer scale and their water contents should be more similar to the mesostasis one, in the range of few wt.% H_2O. Indeed, such inclusions should appear on our NanoSIMS images of AlO^-/Si^-, MgO^-/Si^- and OH^-/Si^-, as we have a resolution down to 100 nm at 1.2 pA. We do not observe any variations in these three ratios during the duration of our analyses, meaning that we do not cross any glass inclusions of this type.

We propose that type I chondrules precursors could be composed of glassy grains, clays minerals or altered ferromagnesians, i.e. hydrous matrix-like material. These precursors would have been incompletely degassed after chondrule cooling and before incorporation into the parent body. Water should have been incorporated into chondrules before their accretion into the parent body, as it seems unrealistic to add a large amount of water in chondrule olivines at parent body conditions.

5.3. Open questions

The Rayleigh distillation model seems to indicate that chondrules would have degassed their primordial hydrogen, distinct from the alteration water, resulting from reduction of water into H_2 at $\simeq$ 900°C. Still, there are some interesting unsolved issues:

(i) The primordial source of hydrogen in chondrules is unknown. The hydrogen isotopic ratio of this source could be as low as -398‰, i.e. the lower δD value measured in chondrule phases. This value is markedly distinct from both the nebula H_2 and the mean chondrite

hydrogen isotopic signature. There are few components with such low δD among solar system objects. The unique organic matter contained in the Abee meteorite in one of them (Remusat et al. 2012; Yang and Epstein 1983). This material signs the occurrence, in the early solar system, of a H-reservoir that was at isotopic equilibrium with molecular H_2 in the neutral environment (Lécluse and Robert, 1994). This source of H could also be responsible of the end-member δD value advocated to interpret the linear variations observed at the scale of the bulk CCs in a D/H vs. C/H diagram: at C/H=0, δD= -444±23‰ (Alexander et al., 2012). According to the present study, in bulk CCs, organic free minerals (chondrules) could be the carriers of a H-reservoir with a low δD.

(ii) This model implies that NAMs had a higher water concentration before the distillation since H_2 was lost from chondrule. Therefore chondrule precursors were hydrated before their melting/crystallization into the form of chondrules and were incompletely outgassed during the rapid cooling of the chondrules. Incorporation of high water content could have been achieved because chondrule precursors included hydroxylated minerals.

It should be emphasized that the presently proposed distillation model does not preclude a late alteration (hydration) of chondrules by circulating parent body water causing a limited homogenization of the initial chondrule δD values. Indeed, - if the fluid was isotopically homogenous – the isotope fractionation between minerals and water is limited to 50 ‰ and thus should not have significantly altered the observed chondrule δD distribution that spars over 764‰.

Acknowledgements

We are grateful to B. Zanda and to the meteorite collection of the Muséum National d'Histoire Naturelle for providing samples of Paris, Renazzo and Bishunpur. We also thank P. Cartigny, E. Deloule and K. Koga for providing standards. We thank the reviewers and the associate editor A.N. Krot for helpful discussion and comments. The National NanoSIMS facility at the Muséum National d'Histoire Naturelle was established by funds from the CNRS, Région Île de France, Ministère délégué à l'Enseignement supérieur et à la Recherche, and the Muséum itself**.**

References

Alexander C.M.O.D., Barber D.J., and Hutchison R. (1989) The microstructure of Semarkona and Bishunpur. *Geochim. Cosmochim. Acta* **53**, 3045-3057.

Alexander C.M.O.D., Bowden R., Fogel M.L., Howard K.T., Herd C.D.K. and Nittler L.R. (2012) The Provenances of Asteroids, and Their Contributions to the Volatile Inventories of the Terrestrial Planets. *Science* **337**, 721-723.

Alexander C.M.O.D., Howard K.T., Bowden R., and Fogel M.L. (2013) The classification of CM and CR chondrites using bulk H, C and N abundances and isotopic compositions. *Geochim. Cosmochim. Acta* **123**, 244-260.

Alexander C.M.O.D., Newsome S.D., Fogel M.L., Nittler L.R., Busemann H., and Cody G.D. (2010) Deuterium enrichments in chondritic macromolecular material—Implications for the origin and evolution of organics, water and asteroids. *Geochim. Cosmochim. Acta* **74**, 4417-4437.

Aubaud C., Withers A.C., Hirschmann M.M., Guan Y., Leshin L.A. Mackwell S.J. and Bell D.R. (2007) Intercalibration of FTIR and SIMS for hydrogen measurements in glasses and nominally anhydrous minerals. *Amer. Mineral.* **92**, 811-828.

Beck P., Quirico E., Montes-Hernandez G., Bonal L., Bollards J., Orthous-Daunay F.-R., Howard K.T., Schmitt B., Brissaud O., Deschamps F., Wunder B. and Guillot S. (2010) Hydrous mineralogy of CM and CI chondrites from infrared spectroscopy and their relationship with low albedo asteroids. *Geochim. Cosmochim. Acta* **74**(16), 4881-4892.

Bell D.R. and Rossman G.R. (1992) Water in Earth's mantle: the role of nominally anhydrous minerals. *Science* **255**, 1391-1397.

Bell D.R. and Rossman G.R. (2003) Hydroxide in olivine: a quantitative determination of the absolute amount and calibration of the IR spectrum. *J. Geophys. Res.* **108**, 1978-2012.

Beran A. and Libowitzky E. (2006) Water in natural mantle minerals II: olivine, garnet and accessory minerals. *Rev. Mineral. Geochem.* **62**, 169-191.

Bischoff A. (1998) Aqueous alteration of carbonaceous chondrites: evidence for preaccretionary alteration. A review. *Meteorit. Planet. Sci.* **33**, 1113-1122.

Boato G. (1954) The isotopic compositionof hydrogen and carbon in the carbonaceous chondrites. *Geochim. Cosmochim. Acta* **6**, 209-220.

Bolfan-Casanova N. (2005) Water in the Earth's mantle. *Mineral. Mag.* **69**, 229-257.

Bonal L., Alexander C.M.O.D., Huss G.R., Nagashima K. and Quirico E. (2013) Hydrogen isotopic composition of the water in CR chondrites. *Geochim. Cosmochim. Acta* **106**, 111-133.

Brearley A.J. (2003) Nebular versus Parent-body processing, in *Meteorites, Comets and Planets: Treatise in Cosmochemistry vol.1* (eds. Davis A.M., Holland, H.D. and Turekan, K.K.) Elsevier–Pergamon, Oxford.

Browning L.B., McSween H.Y. and Zolensky M.E. (1996) Correlated alteration effects in CM carbonaceous chondrites. *Geochim. Cosmochim. Acta* **60**, 2621-2633.

Ciesla F.J., Lauretta D.S., Cohen B.A. and Hood L.L. (2003) A Nebular Origin for Chondritic Fine-Grained Phyllosilicates. *Science* **299**, 549-552.

Clayton R. N. and Mayeda T. K. (1999) Oxygen isotope studies of carbonaceous chondrites. *Geochim. Cosmochim. Acta* **63**, 2089– 2104.

Clog M. (2010) Concentration et composition isotopique de l'hydrogène dans le manteau terrestre. *Ph.D. thesis*.

de Lew S., Rubin A.E., Schmitt A.K. and Wasson J.T. (2009) 53Mn-53Cr systematics of carbonates in CM chondrites: implications for the timing and duration of aqueous alteration. *Geochim. Cosmochim. Acta* **73**, 7433-7442.

Deloule E., France-Lanord C. and Albarède F. (1991) D/H analysis of minerals by ion probe in *Stable isotope Geochemistry : a tribute to Samuel Epstein* (eds Taylor H.P., O'Neil J.R. and Kaplan I.R.) *Geochem. Soc. Spec. Publ.* **3**, 53-62

Deloule E. and Robert F. (1995) Interstellar water in meteorites? *Geochim. Cosmochim. Acta* **59**, 4695-4706.

Deloule E., Robert F. and Doukhan J.C. (1998) Interstellar hydroxyl in meteoritic chondrules: Implications for the origin of the water in the inner solar system. *Geochim. Cosmochim. Acta* **62**, 3367-3378.

Eiler J.M. and Kitchen N. (2004) Hydrogen isotope evidence for the origin and evolution of the carbonaceous chondrites. *Geochim. Cosmochim. Acta* **68**(6), 1395–1411.

Férot A. and Bolfan-Casanova N. (2012) Water storage capacity in olivine and pyroxene to 14GPa: implications for the water content of the Earth's upper mantle and nature of seismic discontinuities. *Earth Planet. Sci. Lett.* **349-350**, 218-230.

Fieni C., Bourot-Denise M., Pellas P. and Touret J. (1978) Aqueous fluid inclusions in feldspars and phosphates from Peetz chondrite. *Meteoritics* **13**, 460.

Florentin L., Faure F., Tissandier L., Deloule E. and Lequin D. (2016) Heated olivine-hosted glass inclusions from Allende CV3 meteorite: insight on chondules origin. *47th Lun. Planet. Sci. Conf.* #1863.

Fujiya W., Sugiura N., Hotta H., Ichimura K. and Sano Y. (2012) Evidence for the late formation of hydrous asteroids from young meteoritic carbonates. *Nature Commun.* **3**, 1-6.

Garenne A., Beck P., Montes-Hernandez G., Chiriac R., Toche F., Quirico E., Bonal L. and Schmitt B. (2014) The abundance and stability of "water" in type 1 and 2 carbonaceous chondrites (CI, CM and CR). *Geochim. Cosmochim. Acta* **137**, 93-112.

Greenwood R.C., Franchi I.A., Pont S., Lorand J.-P., Cournède C., Gattacceca J., Rochette P., Kuga M., Marrocchi Y. and Marty B. (2014) The Paris meteorite, the least altered CM chondrite so far. *Geochim. Cosmochim. Acta* **124**, 190-222.

Guo W. and Eiler J. M. (2007) Temperatures of aqueous alteration and evidence for methane generation on the parent bodies of the CM chondrites. *Geochim. Cosmochim. Acta* **71**, 5565–5575.

Hanowski N.P. and Brearley A.J. (2001) Aqueous alteration of chondrules in the CM carbonaceous chondrite, Allan Hills 81002: implications for parent body alteration. *Geochim. Cosmochim. Acta* **65**, 495-518.

Hauri E.H., Gaetani G.A. and Green T.H. (2006) Partitioning of water during melting of the Earth's upper mantle at H2O-undersaturated conditions. *Earth Planet. Sci. Lett.* **248**, 715–734

Hewins R.H., Bourot-Denise M., Zanda B., Leroux H., Barrat J.-A., Humayun M., Göpel C.,

Hirschmann M.M., Aubaud C. and Withers A.C. (2005) Storage capacity of H_2O in nominally anhydrous minerals in the upper mantle. *Earth Planet. Sci. Lett.* **236**, 167-181.

Howard K.T., Benedix G.K., Bland P.A. and Cressey G. (2011) Modal mineralogy of CM chondrites by X-ray diffraction (PSD-XRD): Part 2. Degree, nature and settings of aqueous alteration. *Geochim. Cosmochim. Acta* **75**, 2735-2751.

Hu S., Lin Y., Zhang J., Hao J., Yang W. and Deng L. (2015) Measurements of water content and D/H ratio in apatite and silicate glasses using a NanoSIMS 50L. *J. Analyt. Atom. Spec.* **30**, 967-978.

Ingrin J. and Blanchard M. (2006) Diffusion of hydrogen in minerals. *Rev. Mineral. Geochem.* **62**, 291-320.

Kerridge J.F. (1985) Carbon, hydrogen and nitrogen in carbonaceous chondrites: Abundances and isotopic compositions in bulk samples. *Geochim. Cosmochim. Acta* **49**, 1707-1714.

Khisina N.R., Wirth R., Andrut M. and Ukhanov A.V. (2001) Extrinsic and intrinsic mode of hydrogen occurrence in natural olivines: FTIR and TEM investigation. *Phys. Chem. Min.* **28**, 291-301.

Koga K., Hauri E., Hirschmann M. and Bell D. (2003) Hydrogen concentration analyses using SIMS and FTIR : comparions and calibration for nominally anhydrous minerals. *Geochem. Geoph. Geosys.* **4**(2).

Kohlstedt D.L., Keppler H. and Rubie D.C. (1996) Solubility of water in the α, β and γ phases of $(Mg,Fe)_2SiO_4$. *Contrib. Mineral. Petrol.* **123**, 345-357.

Kyser T.K. and O'Neill J.R. (1984) Hydrogen isotope systematics of submarine basalts. *Geochim. Cosmochim. Acta* **48**, 2123-2133.

Lécluse C. and Robert F. (1994) Hydrogen isotope exchange reaction rates : origin of water in the inner solar system. *Geochim. Cosmochim. Acta* **58**(13), 2927–2939.

Lécuyer C., Gillet P. and Robert F. (1998) The hydrogen isotope composition of seawater and the global water cycle. *Chem. Geol.* **145**(3–4), 249-261.

Libourel G. and Krot A.N. (2007) Evidence for the presence of planetesimal material among the precursors of magnesian chondrules of nebular origin. *Earth Planet. Sci. Lett.* **254**, 1-8.

Marrocchi Y., Gounelle M., Blanchard I., Caste F. and Kearsley T. (2014) The Paris CM chondrite: Secondary minerals and asteroidal processing. *Meteorit. Planet. Sci.* **49**(7), 1232-1249.

Martin R.F. and Donnay G. (1972) Hydroxyl in the mantle. *Amer. Mineral.* **57**, 554-570.

Marty B. (2012) The origins and concentrations of water, carbon, nitrogen and noble gases on Earth. *Earth Planet. Sci. Lett.* **313-314**, 56-66.

Mosenfelder J.L., Le Voyer M., Rossman G.R., Guan Y., Bell D.R., Asimow P.D. and Eiler J.M. (2011) Analysis of hydrogen in olivine by SIMS: evaluation of standards and protocol. *Amer. Mineral.* **96**, 1725-1741.

Ohtani E., Toma M., Litasov K., Kubo T. and Suzubi A. (2001) Stability of dense hydrous magnesium silicate phases and water storage capacity in the transition zone and lower mantle. *Phys. Earth Planet. Int.* **124**, 105-117.

552 Peslier A.H. (2010) A review of water contents of nominally anhydrous natural minerals in the mantles of
553 Earth, Mars and the Moon. *J. Volcanol. Geotherm. Res.* **197**, 239-258.
554 Piani L., Robert F. and Remusat L. (2015) Micron-scale D/H heterogeneity in chondrite matrices: A
555 signature of the pristine solar system water? *Earth Planet. Sci. Lett.* **415**, 154-164.
556 Rauch M. and Keppler H. (2002) Water solubility in orthopyroxene. *Contrib. Mineral. Petrol.* **143**, 525-
557 536.
558 Remusat L., Rouzaud J.N., Charon E., Le Guillou C., Guan Y. and Eiler J.M. (2012) D-depleted organic
559 matter and graphite in the Abee enstatite chondrite. *Geochim. Cosmochim. Acta* **96**, 319-335.
560 Robert F. (2003) The D/H ratio in chondrites. *Space Sci. Rev.* **206**, 87-101.
561 Robert F. (2006) Solar System Deuterium/Hydrogen Ratio, in *Meteorites and the Early Solar System II*
562 (eds. Lauretta D.S. and McSween H.Y.) University of Arizona Press.
563 Rubin A.E., Trigo-Rodríguez J.M., Huber H., Wasson J.T. (2007) Progressive aqueous alteration of CM
564 carbonaceous chondrites. *Geochim. Cosmochim. Acta* **71**, 2361-2382.
565 Saccocia P.J., Seewald J.S. and Shanks III W.C. (2009) Oxygen and hydrogen isotope fractionation in
566 serpentine-water and talc-water systems from 250 to 450 °C, 50MPa. *Geochim. Cosmochim. Acta* **73**,
567 6789-6804.
568 Simon L., Lécuyer C., Martineau F. and Robert F. (2011) Experimental qtudy of D/H fractionation
569 between water and hydrogen gas during the oxidation of Fe-bearing silicates at high temperatures (600 °C
570 - 1200 °C). *Cent. Euro. Geol.* **54**, 81-93.
571 Skogby H. (2006) Water in natural matle minerals I: pyroxenes. Revi. Mineral. Geochem. **62**, 155-167.
572 Skogby H., Bell D.R. and Rossman G.R., 1990. Hydroxide in pyroxenes: variations in the natural
573 environment. *Amer. Mineral.* **75**, 764-774.
574 Smyth J.R., Frost D.J., Nestola F., Holl C.M. and Bromiley G. (2006) Olivine hydration in the deep upper
575 mantle: effects of temperature and silica activity. *Geophys. Res. Lett. 33*, L15301.
576 Stephant A., Remusat L., Thomen A. and Robert F. (2014) Reduction of OH contamination in
577 quantification of water contents using NanoSIMS imaging. *Chem. Geol. 380*, 20-26.
578 Sundvall R. and Stalder R. (2011) Water in upper mantle pyroxene megacrysts and xenocrysts: a survey
579 study. *Amer. Mineral.* **96**, 1215-1227.
580 Tenner T.J., Hirschmann M.M., Withers A.C. and Hervig R.L. (2009) Hydrogen partitioning between
581 nominally anhydrous upper mantle minerals and melt between 3 and 5 GPa and applications to hydrous
582 peridotite partial melting. *Chem. Geol.* **262**, 42-56.
583 Thomen A., Robert, F. and Remusat L. (2014) Determination of the nitrogen abundance in organic
584 materials by NanoSIMS quantitative imaging. *J. Analyt. Atom. Spec.* **29,** 512-519.
585 Van Schmus W.R. and Wood J.A. (1967) A chemical-petrologic classification for the chondritic
586 meteorites. *Geochim. Cosmochim. Acta* **31**, 747-765.
587 Varela M.E., Kurat G., Hoppe P. and Brandstätter F. (2002) Chemistry of glass inclusions in olivines of
588 the CR chondrites Renazzo, Acfer 182, and El Djouf 001. *Geochim. Cosmochim. Acta* **66**(9), 1663-1679,
589 Veblen D.R. and Buseck P.R. (1981) Hydrous pyriboles and sheet silicates in pyroxenes and uralites:
590 intergrowth microstructures and reaction mechanisms. *Amer. Mineral.* **66**, 1107-1134.
591 Walsh K.J., Morbidelli A., Raymond S.N., O'Brien D.P. and Mandell A.M. (2011) A low mass for Mars
592 from Jupiter's early gas-driven migration. *Nature* **475**, 206-209.
593 Weisberg M.K., Prinz M., Clayton R.N. and Mayeda T.K. (1993) The CR (Renazzo-type) carbonaceous
594 chondrite group and its implications. *Geochim. Cosmochim. Acta* **57**, 1567-1586.
595 Wright K. (2006) Atomistic models of OH defects in nominally anhydrous minerals. *Rev. Mineral.*
596 *Geochem.* **62**, 67-83.
597 Yang J. and Epstein S. (1983) Interstellar organic matter in meteorites. *Geochim. Cosmochim. Acta* **47**,
598 2199-2216.
599 Young E.D., Ash R.D., Philip E. and Rumble III D. (1999) Fluid flow in chondritic parent bodies:
600 deciphering the compositions of planetesimals. *Science* **286**, 1331-1335.

Zolensky M.E., Bodnar R.J., Gibson E.K., Nyquist L.E., Reese Y., Shih C.-Y. and Wiesmann H. (1999) Asteroidal Water Within Fluid Inclusion-Bearing Halite in an H5 Chondrite, Monahans. *Science* **285**, 1377-1379.

Figure captions

Figure 1: SEM images of 12 type I chondrules in Paris from the section with epoxy - Chondrules 1, 19 and 27: barred olivine. Chondrule 19 exhibits a well-preserved glassy mesostasis. Chondrule 4: radial pyroxene. Others chondrules are porphyritics. They presented various stages of aqueous alteration. Some of them like chondrule 6 or D exhibit well-preserved Fe grains, sign of low aqueous alteration. In the other hand, chondrule 27 has its mesostasis transformed into phyllosilicates and an aqueous alteration rim grew around him.

Figure 2: OH^-/Si^- vs H_2O/SiO_2 (ppm/wt.%) calibration for the quantification of water contents. Dashed lines are regression lines calculated with the R program.

Figure 3: Water content distribution in olivine and pyroxene chondrule minerals of Renazzo, Bishunpur and Paris chondrites. Y axis represents the cumulate number of analyses.

Figure 4: Distribution of δD values in the olivines, pyroxenes and mesostases of Renazzo, Bishunpur and Paris chondrules.

Figure 5: NanoSIMS images of an area (20×20µm²) of Paris chondrule A. (a) $^{27}Al^{16}O^-$ image permits to distinguish mesostasis (Mes) and olivine (Ol). (b) D^-/H^- ratio image. We defined ROIs for each phase (blue lines) that fit in both images. The ROI is chosen smaller than the phases due to the different image resolution and the possible shifting occurring between the elemental images and the isotopic image.

Figure 6 : Fractionation coefficients between olivine and mesostasis versus pyroxene and mesostasis reported in per mil. Black square symbols represent our analyses and gray square symbols stand for the distillation numerical simulation explained in section 4.2.3. Arrows indicate direction of fractionation for hydrous alteration of the Paris chondrules, which is unidirectional. The direction will depend on the alteration parameters.

Table captions

Table 1 – EMPA analyses of olivines and pyroxenes from 6 Paris chondrules.

Table 2 – Chemical compositions of standards: (a) from Koga et al. (2003), (b) from Clog (2010), (c) from Deloule et al. (1991).

Table 3 – NanoSIMS data of water concentrations and hydrogen isotopic ratios (expressed in δD) of mesostases, olivines and pyroxenes from 3 Renazzo chondrules (session IV), 4 Bishunpur chondrules (session IV) and 12 Paris chondrules (session III). For sessions II and III, the water concentrations are not

636 reported in the table because the data were obtained at low primary beam intensity and background
637 correction could not be done.

638

(wt.%)	MgO	Al_2O_3	SiO_2	K_2O	CaO	TiO_2	Cr_2O_3	MnO	FeO	NiO	Total	Fa	Fs	Wo
Chondrule 27														
Olivine	54	0	41.4	0	0.2	0.02	0.44	0.15	1.11	0.04	97.6	1.2		
Olivine	54.2	0	40.8	0	0.22	0.02	0.55	0.2	1.01	0.06	97.2	1.1		
Pyroxene	31.3	1.2	45.3	0.04	0.78	0.22	1.8	0.17	11.87	1.32	100.9		17.5	0.4
Pyroxene	34.2	0.8	51.9	0	0.8	0.27	0.61	0.2	2.53	0.08	91.9		3.9	1.6
Chondrule 19														
Olivine	54.3	0.2	42.3	0	0.29	0.03	0.13	0.08	0.8	0.02	98.3	0.8		
Pyroxene	37.5	1.2	57	0	0.47	0.19	0.4	0.08	0.97	0.09	97.9		1.4	0.9
Pyroxene	47.9	0.5	46.8	0.01	0.24	0.1	0.37	0.14	1.56	0.03	97.9		1.8	0.4
Chondrule 4														
Pyroxene	36.3	0.6	55.7	0.01	0.62	0.08	0.85	0.26	1.77	0	96.4		2.6	1.2
Pyroxene	33.8	0.7	53.4	0.02	0.71	0.11	1.59	0.27	5.33	0.32	97.3		8.0	1.4
Chondrule 24														
Olivine	54.6	0.2	41.1	0.01	0.58	0.1	0.34	0.09	0.87	0	98	0.9		
Olivine	54.6	0.2	40.8	0	0.5	0.07	0.24	0	0.89	0	97.4	0.9		
Pyroxene	35.9	2.2	56.5	0.02	1.78	0.3	0.55	0	0.44	0	97.8		0.7	3.4
Pyroxene	34.1	2.9	56.6	0	2.99	0.3	0.56	0.07	0.63	0.02	98.2		1.0	5.9
Pyroxene	21.7	2	52.7	0	18.86	1.01	0.53	0.14	0.36	0.06	97.5		0.6	38.3
Chondrule 6														
Olivine	52.1	0.1	40.6	0	0.47	0.05	0.43	0.17	1.38	0.05	95.8	1.5		
Olivine	54.6	0	41.2	0.02	0.19	0	0.53	0.13	1.46	0.12	98.3	1.5	3.6	1.0
Pyroxene	37.6	1.3	56.8	0.02	0.54	0.27	0.4	0	0.88	0.05	98.1		1.3	1.0
Pyroxene	38.2	1.3	53.6	0	0.55	0.2	0.5	0.15	2.6	0.17	97.5			
Chondrule 9														
Olivine	54.4	0.1	40.9	0	0.31	0.11	0.46	0.14	1.2	0.03	97.8	1.2		
Olivine	54.5	0.1	41.2	0	0.31	0.01	0.48	0.12	1.61	0.07	98.4	1.6		
Pyroxene	32.5	2.1	50.7	0.03	0.97	0.25	0.81	0.25	6.84	0.04	95.3		10.4	1.9
Pyroxene	35.1	2	54.1	0.01	0.99	0.14	0.71	0.11	3.2	0.01	96.6		4.8	1.9
Pyroxene	30	0.5	47.7	0.01	1.2	0.13	1.61	0.37	4.13	0.04	85.9		7.0	2.6

639

640 Table 1

641

	H_2O (ppm)	δD (‰)	SiO_2 (wt.%)	Al_2O_3 (wt.%)	FeO (wt.%)	MnO (wt.%)	MgO (wt.%)	CaO (wt.%)	Na_2O (wt.%)	K_2O (wt.%)	Cr_2O_3 (wt.%)	TiO_2 (wt.%)	P_2O_5 (wt.%)	Cl (wt.%)	Total (%)
Olivine [(a)]															
KLV-23	120	-	40.32	0.05	12.27	-	47.47	0.08	0,03	-	-	0.03	-	-	100.26
Pyroxene [(a)]															
KBH-1	186	-	54.68	4.73	5.88	-	32.92	0.86	0.12	-	-	0.11	-	-	99.32
Glasses [(b)]															
DR15-2-5	2581	-74	50.81	14.78	11.15	0.20	6.95	10.37	3.10	0.46	-	1.82	0.21	0.02	99.85
DR20-1-1	3988	-61	50.20	15.13	10.95	0.20	6.89	10.82	3.07	0.28	-	1.92	0.28	0.03	99.74
Amphiboles [(c)]															
Mt Emma	14300	-50	40.87	13.96	9.84	0.08	14.32	10.79	2.56	1.55	0.09	2.89	-	0.04	98.51
Kipawa	14500	-88	45.05	8.32	12.77	0.24	14.01	10.90	2.48	1.05	0.05	0.80	-	0.59	98.49

642

643 Table 2

644

645

646

647

648

649

650

651

652

653

654

Chondre	Phase	δD (‰)	H_20 (ppm)
Renazzo			
Session IV			
Chondrule X	mesostasis	-73 ± 146	-
	mesostasis	-81 ± 150	2284 ± 275
	olivine	-139 ± 132	115 ± 58
	mesostasis	15 ± 156	-
	pyroxene	-116 ± 137	366 ± 183
Chondrule Y	olivine	-188 ± 129	182 ± 91
	olivine	-115 ± 150	196 ± 98
	mesostasis	-212 ± 125	-
	mesostasis	-211 ± 121	32373 ± 3899
	pyroxene	-109 ± 142	1481 ± 740
	pyroxene	-120 ± 140	1407 ± 703
Chondrule Z	olivine	-192 ± 126	158 ± 79
	pyroxene	-161 ± 132	320 ± 160
	olivine	-120 ± 128	133 ± 67
	olivine	-125 ± 137	215 ± 108
	olivine	-148 ± 132	94 ± 47
	surrounding matrix	316 ± 202	-
Bishunpur			
Session IV			
Chondrule I	mesostasis	-166 ± 133	4702 ± 566
	olivine	-30 ± 151	121 ± 61
	olivine	-164 ± 137	159 ± 79
	mesostasis	-53 ± 146	4725 ± 569
	olivine	-149 ± 135	399 ± 199
	olivine	0 ± 156	159 ± 79
	pyroxene	52 ± 163	659 ± 330
	pyroxene	137 ± 176	1244 ± 622
	surrounding matrix	-113 ± 136	-
Chondrule J	pyroxene	-60 ± 145	1328 ± 664
	pyroxene	-118 ± 138	1796 ± 898
	pyroxene	-149 ± 131	1395 ± 698
	pyroxene	-81 ± 143	674 ± 337
	olivine	-115 ± 136	76 ± 38
	pyroxene	-95 ± 152	649 ± 324
	surrounding matrix	-119 ± 136	-
Chondrule K	olivine	-36 ± 148	-

	pyroxene	-18 ± 153	-
	mesostasis	-46 ± 148	-
Chondrule L	mesostasis	-122 ± 138	5641 ± 679
	pyroxene	-44 ± 149	1090 ± 545
	mesostasis	-49 ± 148	15107 ± 1819
	pyroxene	20 ± 159	567 ± 284
	olivine		316 ± 158
	olivine		326 ± 163
	pyroxene		0
	pyroxene		266 ± 131

656

657

Chondre	Phase	δD (‰)	H_20 (ppm)
Session I			
Chondrule 4	mesostasis	-129 ± 31	-
	pyroxene	-121 ± 61	-
	mesostasis	-90 ± 31	-
	pyroxene	- 86 ± 31	-
	mesostasis	-104 ± 32	-
	pyroxene	-89 ± 35	-
	surrounding matrix	-94 ± 100	-
Chondrule24	mesostasis	-99 ± 36	-
	pyroxene	-80 ± 43	-
	olivine	19 ± 54	-
	mesostasis	-252 ± 38	-
	olivine	-125 ± 50	-
	pyroxene	-12 ± 44	-
Chondrule 6	mesostasis	-97 ± 30	-
	olivine	-130 ± 35	-
	olivine	18 ± 45	-
	pyroxene	-34 ± 35	-
	surrounding matrix	-27 ± 39	-
Chondrule19	mesostasis	-23 ± 45	-
	olivine	-21 ± 38	-
	olivine	0 ± 46	-
	pyroxene	-91 ± 37	-
Chondrule27	mesostasis	-182 ± 28	-
	olivine	-24 ± 43	-

	mesostasis	-212 ± 27	-
	pyroxene	20 ± 27	-
Chondrule 9	pyroxene	-41 ± 36	-
	mesostasis	64 ± 40	-
	pyroxene	22 ± 41	-
	pyroxene	155 ± 53	-
	surrounding matrix	-77 ± 75	
			-
Paris			
Session II			
Chondrule 1	olivine	-93 ± 28	-
	mesostasis	140 ± 36	-
	mesostasis	115 ± 36	-
	olivine	-66 ± 48	-
	pyroxene	-62 ± 32	-
	mesostasis	37 ± 30	-
	olivine	-213 ± 31	-
	pyroxene	21 ± 45	-
Chondrule 7	mesostasis	-96 ± 26	-
	olivine	-116 ± 30	-
	mesostasis	-132 ± 24	-
	olivine	-36 ± 30	-
	pyroxene	-113 ± 50	-
Paris			
Session III			
Chondrule A	olivine	-374 ± 30	603 ± 145
	olivine	-279 ± 29	758 ± 182
	olivine	-334 ± 31	961 ± 231
	olivine	-179 ± 45	949 ± 228
	mesostasis	-17 ± 25	30720 ± 1516
	mesostasis	-274 ± 18	6175 ± 305
	olivine	-398 ± 23	961 ± 231
	mesostasis	266 ± 119	6470 ± 319
	olivine	76 ± 36	781 ± 188
	pyroxene	-179 ± 25	503 ± 121
	pyroxene	-342 ± 23	985 ± 237
	mesostasis	-175 ± 22	5630 ± 278
Chondrule B	mesostasis		66419 ± 3277
	pyroxene		860 ± 207
	olivine		844 ± 203
	pyroxene		900 ± 216
	olivine		859 ± 206

	olivine		998 ± 240
	mesostasis	101 ± 34	33462 ± 1651
	pyroxene	-225 ± 21	698 ± 168
	pyroxene	-172 ± 22	1174 ± 282
Chondrule D	mesostasis	-102 ± 29	8931 ± 441
	olivine	-225 ± 21	799 ± 182
	mesostasis	-270 ± 21	7940 ±392
	pyroxene	-337 ± 20	595 ± 143
Chondrule E	mesostasis	191 ± 29	87466 ± 4317
	pyroxene	83 ± 27	615 ± 148
	olivine	-172 ± 31	
	mesostasis	112 ± 29	10934 ± 539
	olivine	13 ± 29	1051 ± 253
	mesostasis	366 ± 35	31575 ± 1558
	olivine	-138 ± 27	933 ± 224
	mesostasis	-292 ± 32	15926 ± 786
	olivine	-208 ± 23	905 ± 218
	olivine	-225 ± 29	639 ± 154

Table 3

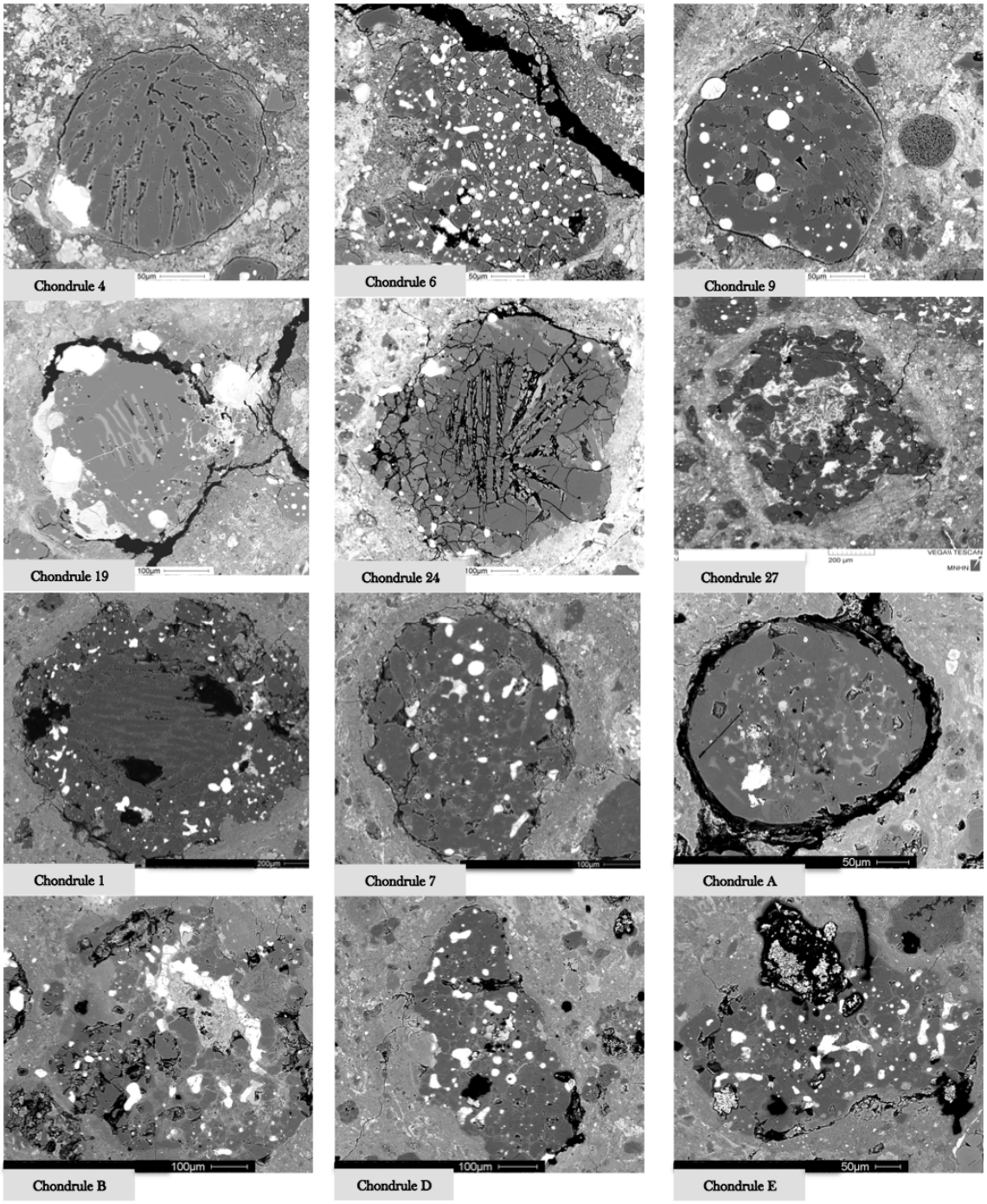

661

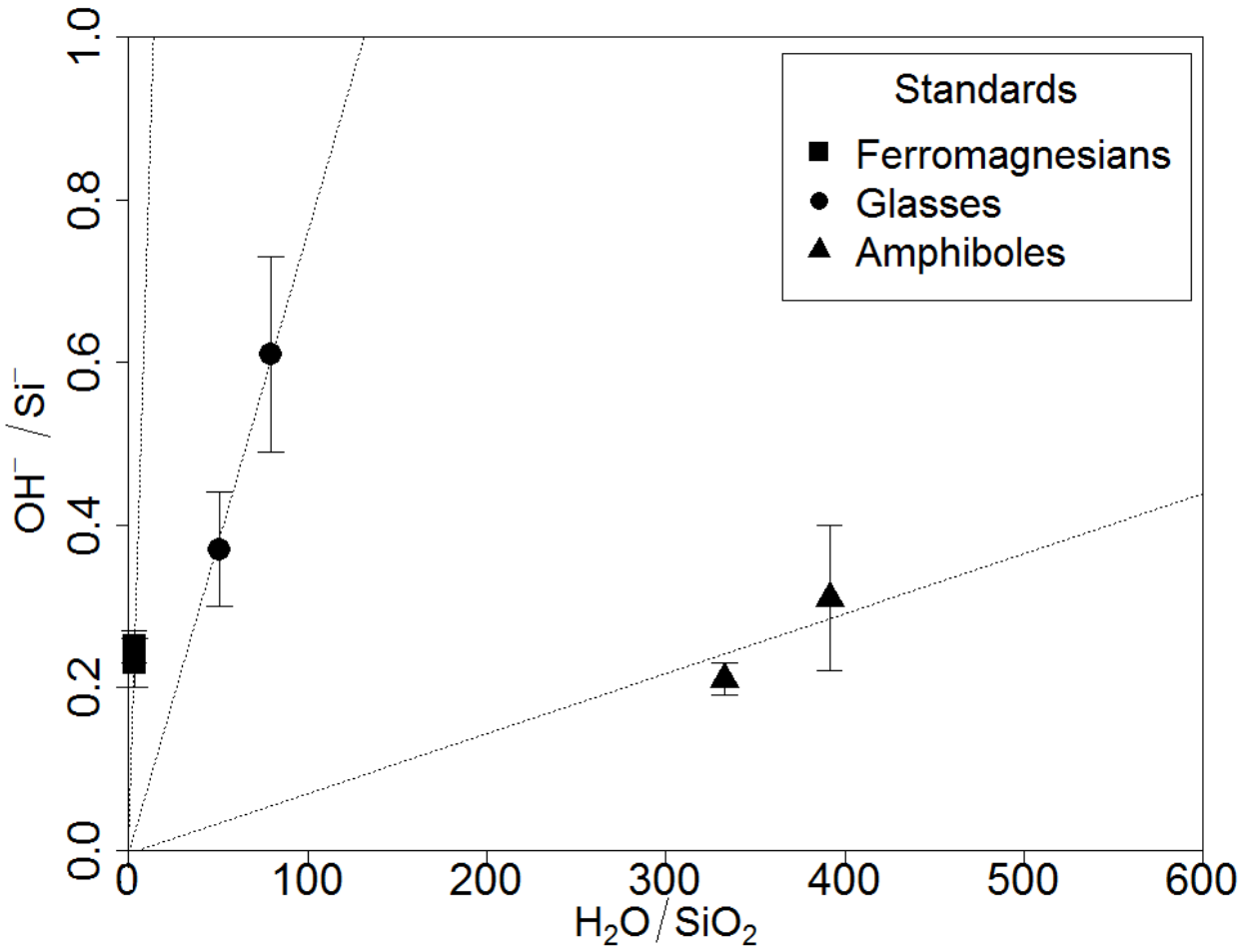

663

664

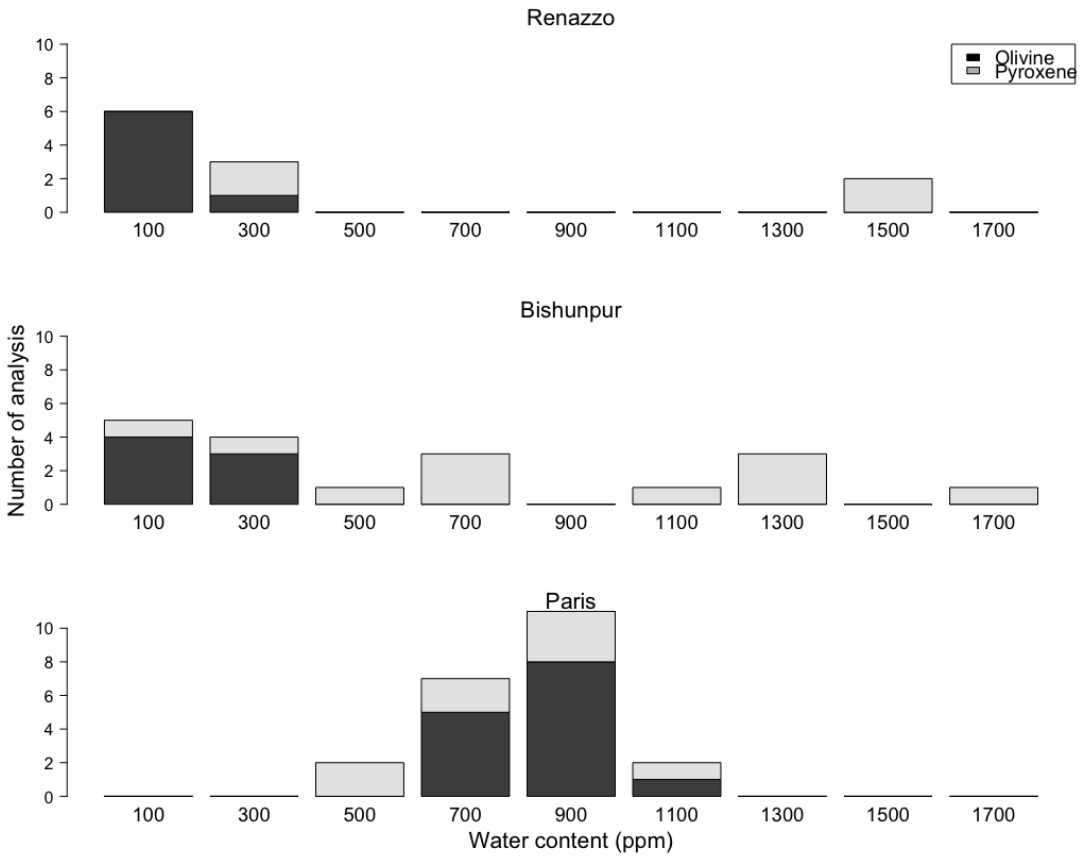

665

666

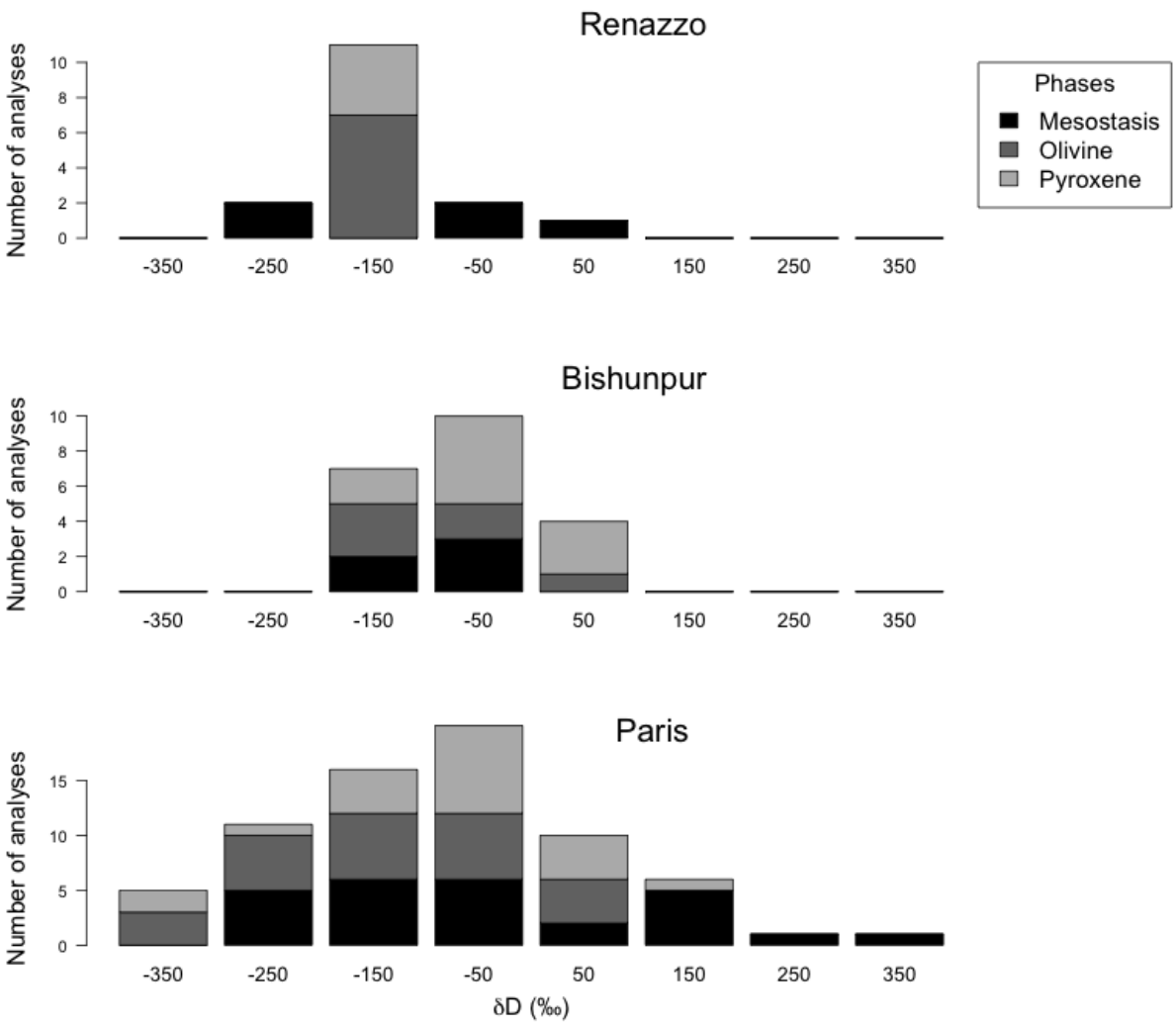

667

668

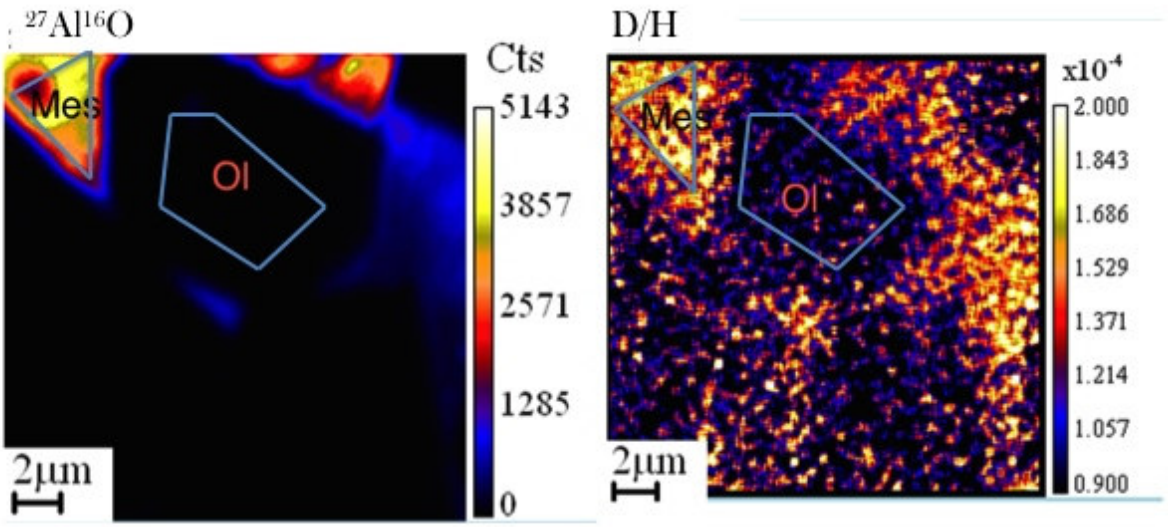

669

670

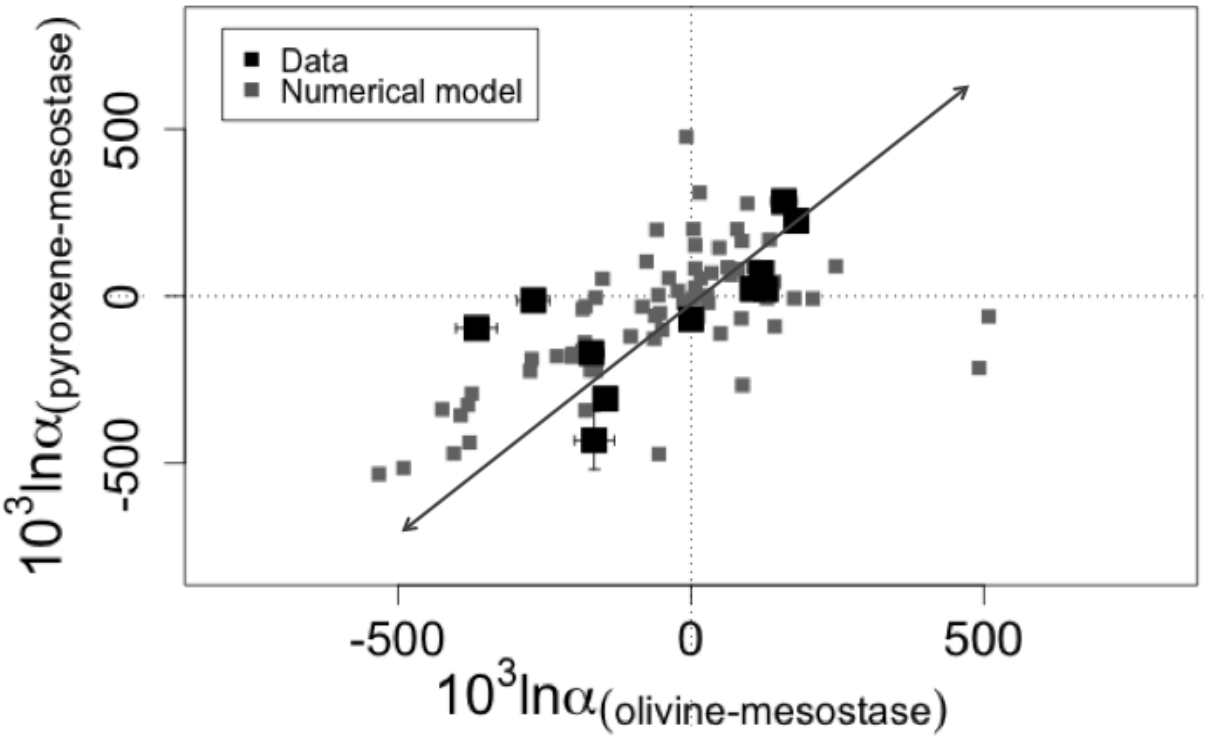

671